Sensors and Materials, Vol. 35, No. 10 (2023) 3731–3741
MYU Tokyo

S & M 3447

Letter

Remote Monitoring of Deep-subwavelength Thickness Variation Using Deformable Metamaterial Absorbers

Shenwei Yin,[1] Xiubo Jia,[2*] Jiawen You,[1] Yuebo Luo,[1] and Zhixiang Tang[1**]

[1]School of Physics and Electronics, Hunan University, Changsha 410082, China
[2]Hunan Engineering Laboratory for Control and Optimization of PV Systems, Hunan Vocational Institute of Technology, Xiangtan 411104, China

(Received December 7, 2022; accepted September 5, 2023)

Keywords: deformable metamaterial absorber, deep subwavelength, thickness monitor

Interferometry, a typical phase-sensitive measurement, usually requires additional hardware and complex signal processing to achieve subwavelength resolution. In this paper, we propose a potential thickness variation monitor, in which only reflection losses are needed to achieve deep-subwavelength accuracy. The proposed monitor is based on a sensitive thickness-dependent metamaterial absorber (MMA), which is made of split copper rings periodically arranged in a flexible and nonabsorbent thermoplastic polyurethane base. Experimental results showed that the frequency of the absorption peak increases almost linearly in the range from 6.655 to 6.755 GHz when the thickness of the MMA decreases from 25.625 to 24.833 mm with a step of 0.0417 mm, about a thousandth of the central wavelength of this frequency region. The effects of two key geometry parameters, i.e., the distance from the split copper ring to the metal base and the gap width of the split copper ring, on the absorption performance are investigated by numerical simulation. Our results may provide a simple method of monitoring deep-subwavelength thickness variation in the far field.

1. Introduction

Metamaterial absorbers (MMAs) have attracted considerable attention since Landy *et al.* first proposed a nearly perfect microwave absorber using metamaterials in 2008,[(1)] owing to their important applications in stealth cover,[(2)] chirality-selective absorption,[(3)] selective thermal emitters,[(4–6)] solar energy harvesting,[(7–11)] and so on. Usually, the structures and sizes of these MMAs are fixed, and the absorption characteristics can no longer be changed, lacking adaptability and tunability.

To make up for this disadvantage, tunable MMAs have been proposed and extensively studied in recent years.[(12–24)] The absorption characteristics of these MMAs can be changed by mechanical stretching,[(18,19)] photoexcitation,[(20)] electrical excitation,[(21)] and other external physical fields.[(22–24)] For example, Li *et al.* demonstrated a resonance-frequency tunable MMA working at terahertz frequencies, which was made of a planar arranged resonator on a highly

*Corresponding author: e-mail: jiaxiubo@xlgy.com
**Corresponding author: e-mail: tzx@hun.edu.cn
https://doi.org/10.18494/SAM4269

ISSN 0914-4935
https://myukk.org/

stretchable substrate.[18] The MMA experimentally showed a large frequency shift with a small applied stretch. Additionally, Su *et al.* proposed a dual-band tunable MMA, in which the geometric parameters of the particularly designed metal structure can be adjusted through the applied pressure.[19] With increasing pressure, the absorption peak at low frequency gradually increases, whereas the other absorption peak at high frequency decreases simultaneously. MMA-based sensors exhibit significant promise owing to their high sensitivity, quality factor, cost-effectiveness, and ease of fabrication, enabling the accurate measurement of physical parameters. Islam *et al.* proposed a digit 8-shaped resonator-inspired metamaterial for measuring the thickness of multilayered structures with an accuracy of 0.5 mm.[25] Using a single-microstrip transmission line with a pair of coupled circular complementary spiral resonators, Sun *et al.* realized a subwavelength planar microwave sensor to measure thickness with an accuracy of 0.1 mm and the permittivity of a dielectric sheet.[26] Here, we propose an MMA made of a flexible base and split-ring resonators, which has potential in monitoring deep-subwavelength thickness variation in the far field.

Usually, to achieve subwavelength accuracy in the measurement, interferometry, which is one of the most effective methods, has been widely used.[27–30] For example, optical interferometry uses light interference to determine thickness with ensured reliability and high precision.[31–33] Compared with the optical-based method, microwave and millimeter-wave interferometries have advantages against harsh environments such as fogs, oils, and powders in practical applications.[34–38] Using microwave integrates and monolithic microwave integrated circuits, Kim and Nguyen realized a millimeter-wave sensor with a resolution of $\lambda_0/840$, where λ_0 is the free space wavelength.[34] Using frequency and phase evaluation algorithms, Ayhan *et al.* developed a frequency-modulated continuous wave radar system for high-accuracy range detection.[36] By combining several continuous wave radars with different operating frequencies, the measurement accuracy of the radar system can be improved further.[37,38]

However, interferometry is a typical phase-sensitive measurement, which usually requires additional hardware and complex signal processing to achieve reliable precision. In this paper, we propose a potential thickness variation monitor with deep-subwavelength accuracy based on the sensitive thickness-dependent absorption of the designed MMA. Experimental results showed that the frequency of the absorption peak increases almost linearly with the decrease in MMA thickness with a step of 0.0417 mm, about a thousandth of the wavelength. The effects of two main geometry parameters of the MMA on the absorption performance have also been investigated by numerical simulation.

2. Structure and Experiment

A unit cell of the proposed MMA is schematically shown in Fig. 1. The unit cells are periodically distributed in a square lattice with a lattice constant at 18 mm in the x- and y-directions. The split resonant ring (SRR), which is made of a split copper ring on top of a hard FR4 plate, is obliquely held by a designed flexible base. When the top of the absorber is pressed downward, the FR4 plate is expected to rotate around the x-axis, and the included angle θ between the SRR and the flexible base decreases, i.e., the thickness of the absorber decreases. The absorption characteristic of the MMA is mainly determined by the magnetic flux passing

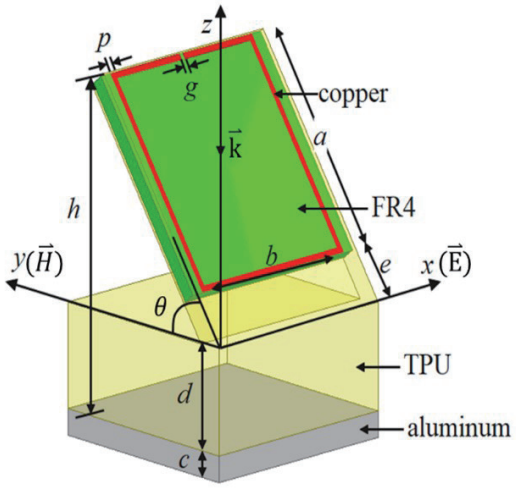

Fig. 1. (Color online) Sketch of a unit cell of proposed MMA.

through the SRR, which is sensitive to the SRR tilt angle. To lengthen the interaction time between the incident electromagnetic wave and the SRR, an aluminum plate is placed at the bottom of the flexible base to totally reflect the incident wave back. The thicknesses of the aluminum plate and flexible base are $c = 2$ and $d = 8$ mm, respectively. The FR4 plate and copper ring are cubic and their thicknesses are 0.8 and 0.035 mm, respectively. The copper ring is fabricated at the center of the FR4 plate, its two side lengths are $a = 18$ and $b = 16$ mm, and its width is $p = 0.5$ mm. The split of the copper ring is on the top side and the width of the gap is $g = 0.1$ mm. The distance between the SRR and the flexible base is $e = 4$ mm. The initial value of θ is 53.24°, so that the thickness of the whole absorber is $h = 25.625$ mm. The relative permittivities of the flexible material and FR4 plate are 1.5 and 4.4, respectively. The incident electromagnetic wave propagates in the negative direction of the z-axis, with the electric and magnetic fields polarized along the x- and y-directions, respectively. Note that the magnetic field is perpendicular to the SRRs, guaranteeing that the induced currents in the split copper rings can be excited effectively.

For fabricating the proposed MMA, we use a 3D printer to print a flexible base with unit cells arranged 10 by 10 on top of an aluminum slab of 180 × 180 × 2 mm^3. The 3D printing material used here is thermoplastic polyurethane (TPU), which is flexible and almost nonabsorbent in the GHz band. To reduce the effective permittivity and enhance the flexibility of the printed base, a low filling ratio of 30% is adopted during the 3D printing process. Then, the SRRs are assembled in the flexible base periodically as shown in the inset of Fig. 2(a). In the upper part of the soft base, a slot structure is printed, and FR4 plates are inserted into it to keep the FR4 plates relatively fixed. Moreover, an acrylic plate with a set of acrylic bolt and nut is fixed with the bottom aluminum plate. The acrylic plate, which is placed on top of the MMA, can move downward or upward by screwing the nut in or out, for changing the thickness of the MMA in the absorption measurement ensuring consistency in the decrease in thickness across all cells, minimizing individual differences and ensuring uniform absorption characteristics throughout the MMA.

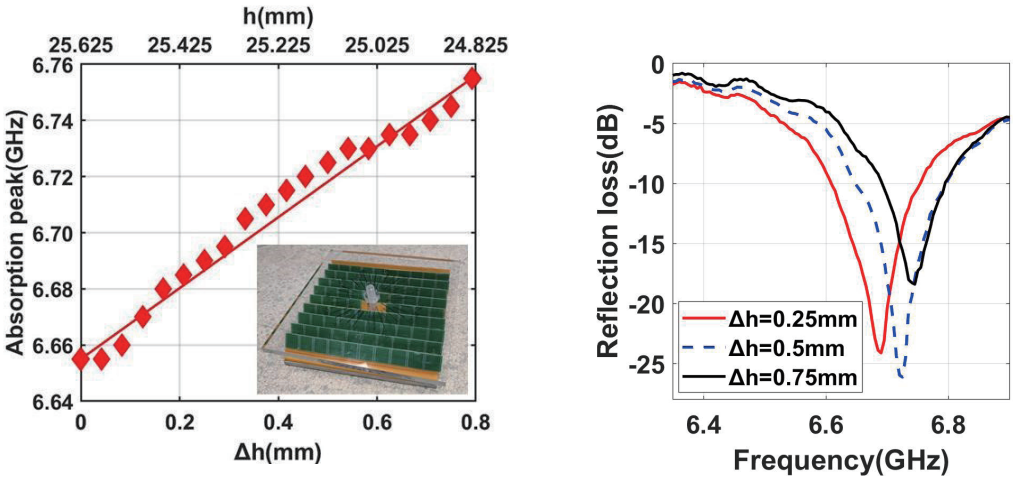

(a) (b)

Fig. 2. (Color online) Experimental results of thickness-dependent absorptions of proposed MMA. (a) Thickness h and thickness decrease Δh vs peak frequency of absorption. The inset is the fabricated MMA. (b) Measured absorptions of fabricated MMA for three Δh values of 0.25, 0.50, and 0.75 mm.

The absorption of the proposed MMA is characterized by reflection loss and measured using a vector network analyzer (CETC41 AV3672B-S). We set 800 points during a linear frequency sweep from 5 to 9 GHz, suggesting a frequency resolution of 0.005 GHz. By screwing the acrylic nut downward with a step of 10°, the MMA thickness h decreases from 25.625 to 24.833 mm with a step of 0.0417 mm. For each thickness decrease, we record the frequency of the absorption peak. The experimentally measured results are shown in Fig. 2(a). Here, we only focus on the absorption in the frequency range from 6.0 to 7.0 GHz because all the absorption peaks in this range are distinct and less than −15 dB. As examples, the absorption spectra for three Δh values of 0.25, 0.50, and 0.75 mm are plotted in Fig. 2(b). Clearly, the absorption peak moves to the high frequency when the thickness of the MMA decreases. More importantly, according to the experimental results, the frequency shift is almost linear with respect to the decrease in thickness, indicating a potential thickness variation monitoring. Furthermore, compared with the central wavelength λ_0 in this frequency range, the step of the experimentally measured thickness change is about $\lambda_0/1100$. To verify the experimental repeatability, three MMAs were fabricated and each of them was subjected to individual experimentation. As shown in Fig. 3, the results obtained clearly demonstrate that all three MMAs exhibit remarkably similar absorption characteristics, showing an approximately linear variation of the absorption peak within a specific frequency range.

3. Theory and Numerical Simulation

For a better understanding of the experiment results, numerical simulation is performed using the 3D finite-difference time-domain (FDTD) method.[39] To mimic a plane wave perpendicularly incident to the proposed MMA, periodic boundary conditions are applied to the

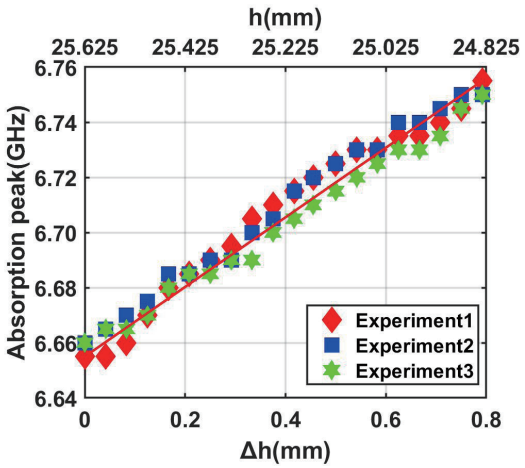

Fig. 3. (Color online) Experimental results of thickness-dependent absorptions of three fabricated MMAs.

four sides of the unit cell, which are perpendicular to the *x*- and *y*-axes, respectively. Moreover, perfect matching layers are employed along the *z*-axis. Moreover, a plane wave source is placed on top of the SRR and a two-dimensional frequency-domain monitor is located behind the source to record the reflected power.

Similar to the experimental measurement, in the numerical simulation, we only consider the absorption of the MMA from 6.0 to 7.0 GHz. The simulation results are plotted (the blue line with squares) and compared with the experimental results (the red line with diamonds) in Fig. 4. It is clearly shown that the peak frequency of the simulated absorption increases linearly with the decrease in MMA thickness, agreeing well with the experimental results except for a slight frequency shift. This difference is mainly caused by two factors. First, a low filling ratio of 30% was taken in the 3D printing process for the soft base, resulting in a slight difference from the simulation. Second, in the frequency range of 1–15 GHz, the relative dielectric constant and loss tangent of the FR4 plate tend to exhibit instability.[40] In the simulation, a relative dielectric constant of 2.4 and a loss tangent of 0.01 were chosen for a frequency of 8.4 GHz based on Ref. 40. However, these simulation values may not precisely match the actual electromagnetic characteristics of the 6.5–7 GHz frequency band in the experiment. Despite these differences, the simulation results still effectively prove the feasibility of the MMA and its properties of approximately linear variation of the absorption peak in a specific frequency range.

For a thorough study, the effects of the geometry parameters of the unit cell on the absorption peak of the MMA have been systematically analyzed. Here, we only consider two key geometry parameters, i.e., the distance *e* between the SRR and the flexible base and the gap width *g* of the SRR. The first one is the main factor in determining the magnetic flux passing through the SRR and the induced current in the SRR. The second one plays an important role in dissipating the electromagnetic waves efficiently. Figure 5 shows the thickness-dependent absorption of the MMA for the distance *e* changing from 1 to 7 mm with a step of 3 mm. It is clear that the distance *e* affects not only the absorption intensity considerably but also the dependence of the peak frequency on the MMA thickness. As shown in Figs. 5(a) and 5(c), all of the simulated

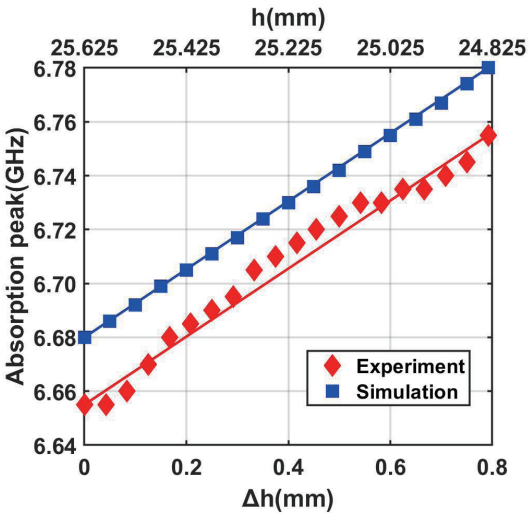

Fig. 4. (Color online) Thickness decrease vs peak frequency of absorption of proposed MMA. The red line with diamonds and the blue line with squares denote the experimental and simulation results, respectively.

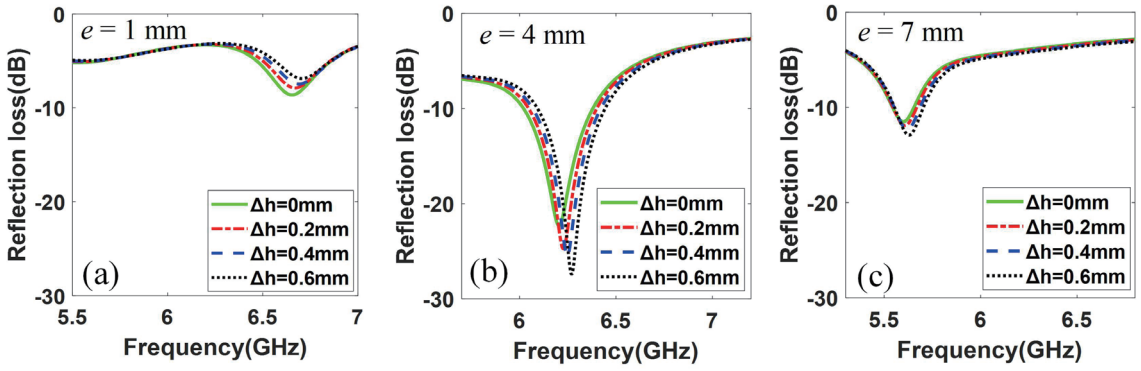

Fig. 5. (Color online) Effect of distance between SRR and soft base on absorption peak: (a) e = 1, (b) e = 4, and (c) e = 7 mm.

maximum absorptions are larger than −15 dB, and the peak frequency is almost invariant with the thickness decrease for e = 1 and 7 mm. However, as presented in Fig. 5(b), for e = 4 mm, the absorption peak moves clearly to the high frequency when the thickness of the MMA decreases. Moreover, all the maximum reflection losses are less than −15 dB, indicating strong and distinguishable absorptions.

Similarly, the effect of the gap width g of the SRR on the absorption is also investigated by numerical simulation. As shown in Fig. 6, for every gap width g, the frequency of the absorption peak increases when the thickness of the MMA decreases. For g = 0.5 and 1 mm, the peak absorptions of the MMAs are clearly weaker than those for g = 0 and 0.1 mm. Comparatively, both the frequency shift of the peak absorption and the maximums of the absorptions are most significant for the gap width g = 0.1 mm.

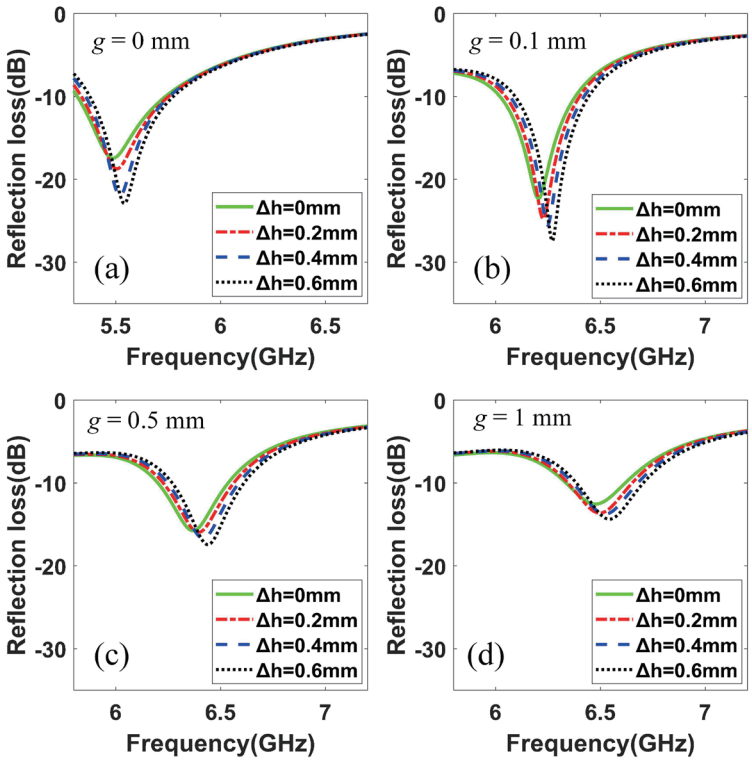

Fig. 6. (Color online) Effect of gap width of SRR on absorption peak: (a) g = 0 (b) g = 0.1, (c) g = 0.5, and (d) g = 1 mm.

Although the absorption mechanism for the MMA is always very complicated, here, we present a simple theoretical model based on the equivalent circuit theory to understand the simulation and experimental results. On the basis of the equivalent circuit theory,[41,42] our deformable absorber can be roughly described by an *RLC* resonant circuit as shown in Fig. 7. The resonance frequency f_m of the MMA can be written as

$$f_m = \frac{1}{2\pi\sqrt{LC}}. \tag{1}$$

For our MMA, the effective capacitance C mainly originates from the resonant ring gap and is almost unchanged during the deformation of the MMA, since the gap width g is invariant and negligible compared with the resonant ring lengths a and b. Therefore, the resonance frequency f_m is primarily determined by the effective inductance L, because the effective resistance is also invariant. As shown in Fig. 1, the magnetic flux through the SRR is given by $\Phi = \int \vec{B} \cdot d\vec{S} \approx BS\sin\theta$, where B and S are the magnetic field and area of the SRR, respectively. For a harmonic incident wave with an angle frequency ω, the induced electric potential difference in the SRR is $V = -d\Phi / dt = j\omega BS\sin\theta$. Moreover, the effective inductance L can be decomposed into two parts, the self-inductance L_s of the SRR and the mutual inductance L_M between the SRR and its image due to the ground metal plane beneath it. Specifically, the SRR

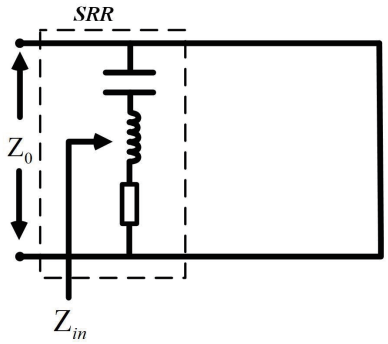

Fig. 7. Equivalent circuit of proposed MMA.

induces an SRR image with the same current given by $I^- = I^+$ because the reflected magnetic field is in the same direction as the incident one. The coupling between the SRR and its image can be expressed in matrix form as

$$\begin{bmatrix} V^+ \\ V^- \end{bmatrix} = j\omega \begin{bmatrix} L_s & L_M \\ L_M & L_s \end{bmatrix} \begin{bmatrix} I^+ \\ I^- \end{bmatrix}, \tag{2}$$

where V^+ and V^-, and I^+ and I^- are the induced voltage and current of the SRR and their images, respectively. It can be readily shown that the eigen solutions of Eq. (2) have the inductance eigen values of $L = L_S + L_M$ and the corresponding eigen vectors $[1, 1]^T$. Finally, substituting $V = j\omega BS\sin\theta$ into Eq. (2), we can see that the effective inductance L decreases as the angle θ decreases, whereas, according to Eq. (1), the resonant frequency increases.

4. Conclusions

We have experimentally demonstrated a deformable MMA, which has potential in the remote monitoring of deep-subwavelength thickness variation. Different from the widely used interferometry, which usually requires additional hardware and complex signal processing to achieve subwavelength resolutions, our proposed method only needs to measure the reflection loss of the MMA. The proposed monitor is based on a very sensitive thickness-dependent MMA, which is made of split copper rings obliquely held by a flexible and nonabsorbent TPU base. The soft TPU base makes the SRR capable of tilting in one direction and reducing its included angle with the TPU base to change the thickness of the MMA. The experimentally measured results showed that the frequency of the absorption peak increases almost linearly in the range from 6.655 to 6.755 GHz when the thickness of the MMA decreases from h = 25.625 to 24.833 mm with a step of 0.0417 mm, about one-thousandth of the central wavelength of this frequency region. Numerical simulation has also been conducted to check this sensitive thickness-dependent absorption. The simulation results agreed well with the experimental results except a frequency shift. This discrepancy may be attributed to the fabrication errors and the introduction of the acrylic parts in the experiments.

Moreover, the effects of two key geometry parameters, i.e., the distance between the split copper ring and the flexible base and the gap width of the split copper ring, on the absorption performance have been investigated by numerical simulation. The simulation results showed that the maximum absorption of the MMA is sensitive to these two parameters. Our results may give a new way to monitor deep-subwavelength thickness variation in the far field. For example, the MMA can be integrated in some mechanical and building structures for the precise and long-term monitoring of the fine variation of their thicknesses in the far field, especially in places that are inaccessible to humans.

Acknowledgments

This research was funded by the Natural Science Foundation of Hunan Province, China (No. 2021JJ60051) and the Scientific Research Foundation of Hunan Education Department (No. 18C1446).

References

1 N. I. Landy, S. Sajuyigbe, J. J. Mock, D. R. Smith, and W. J. Padilla: Phys. Rev. Lett. **100** (2008) 4. https://doi.org/10.1103/PhysRevLett.100.207402
2 Y. Lai, H. Y. Chen, Z. Q. Zhang, and C. T. Chan: Phys. Rev. Lett. **102** (2009) 4. https://doi.org/10.1103/PhysRevLett.102.093901
3 D. B. Stojanović, G. Gligorić, P. P. Beličev, M. R. Belić, and L. Hadžievski: IEEE J. Sel. Top. Quantum Electron. **27** (2021) 6. https://doi.org/10.1109/jstqe.2020.3024570
4 X. L. Liu, T. Tyler, T. Starr, A. F. Starr, N. M. Jokerst, and W. J. Padilla: Phys. Rev. Lett. **107** (2011) 4. https://doi.org/10.1103/PhysRevLett.107.045901
5 F. B. P. Niesler, J. K. Gansel, S. Fischbach, and M. Wegener: Appl. Phys. Lett. **100** (2012) 3. https://doi.org/10.1063/1.4714741
6 H. Wang, J. Y. Chang, Y. Yang, and L. P. Wang: Int. J. Heat Mass Transfer **98** (2016) 788. https://doi.org/10.1016/j.ijheatmasstransfer.2016.03.074
7 Y. Wang, T. Y. Sun, T. Paudel, Y. Zhang, Z. F. Ren, and K. Kempa: Nano Lett. **12** (2012) 440. https://doi.org/10.1021/nl203763k
8 F. Dincer, O. Akgol, M. Karaaslan, E. Unal, and C. Sabah: Prog. Electromagn. Res. **144** (2014) 93. https://doi.org/10.2528/pier13111404
9 J. M. Hao, L. Zhou, and M. Qiu: Phys. Rev. B **83** (2011) 12. https://doi.org/10.1103/PhysRevB.83.165107
10 K. Aydin, V. E. Ferry, R. M. Briggs, and H. A. Atwater: Nat. Commun. **2** (2011) 7. https://doi.org/10.1038/ncomms1528
11 M. A. Baqir and P. K. Choudhury: IEEE Photonics Technol. Lett. **29** (2017) 1548. https://doi.org/10.1109/lpt.2017.2735453
12 N. I. Zheludev and Y. S. Kivshar: Nat. Mater. **11** (2012) 917. https://doi.org/10.1038/nmat3431
13 H. K. Kim, D. Lee, and S. Lim: Sensors **16** (2016) 10. https://doi.org/10.3390/s16081246
14 S. C. Bakshi, D. Mitra, and L. Minz: Plasmonics **13** (2018) 1843. https://doi.org/10.1007/s11468-018-0698-2
15 H. K. Kim, D. Lee, and S. Lim: Appl. Optics **55** (2016) 4113. https://doi.org/10.1364/ao.55.004113
16 M. K. Hedayati, A. U. Zillohu, T. Strunskus, F. Faupel, and M. Elbahri: Appl. Phys. Lett. **104** (2014) 5. https://doi.org/10.1063/1.4863202
17 K. Ling, M. Yoo, W. J. Su, K. Kim, B. Cook, M. M. Tentzeris, and S. Lim: Opt. Express **23** (2015) 110. https://doi.org/10.1364/oe.23.000110
18 J. N. Li, C. M. Shah, W. Withayachumnankul, B. S. Y. Ung, A. Mitchell, S. Sriram, M. Bhaskaran, S. J. Chang, and D. Abbott: Appl. Phys. Lett. **102** (2013) 4. https://doi.org/10.1063/1.4773238
19 X. Su, C. H. Feng, Y. J. Zeng, and H. B. Yu: Opt. Commun. **459** (2020) 6. https://doi.org/10.1016/j.optcom.2019.124885
20 G. C. Wang, J. N. Zhang, B. Zhang, T. He, Y. N. He, and J. L. Shen: Opt. Commun. **374** (2016) 64. https://doi.org/10.1016/j.optcom.2016.04.052

21 L. Liu, L. Kang, T. S. Mayer, and D. H. Werner: Nat. Commun. **7** (2016) 8. https://doi.org/10.1038/ncomms13236
22 W. M. Zhu, A. Q. Liu, X. M. Zhang, D. P. Tsai, T. Bourouina, J. H. Teng, X. H. Zhang, H. C. Guo, H. Tanoto, T. Mei, G. Q. Lo, and D. L. Kwong: Adv. Mater. **23** (2011) 1792. https://doi.org/10.1002/adma.201004341
23 N. T. Hien, L. N. Le, P. T. Trang, B. S. Tung, N. D. Viet, P. T. Duyen, N. M. Thang, D. T. Viet, Y. P. Lee, V. D. Lam, and N. T. Tung: Comput. Mater. Sci. **103** (2015) 189. https://doi.org/10.1016/j.commatsci.2015.02.038
24 B. X. Wang, X. Zhai, G. Z. Wang, W. Q. Huang, and L. L. Wang: Opt. Mater. Express **5** (2015) 227. http://doi.org/10.1364/ome.5.000227
25 M. T. Islam, M. N. Rahman, M. Samsuzzaman, M. F. Mansor, and N. Misran: Sensors **18** (2018) 4213. https://doi.org/10.3390/s18124213
26 H. Sun, H. Deng, P. Meng, S. Wang, Y. Shuai, and Q. Gao: IEEE Sens. J. **22** (2022) 22591. https://doi.org/10.1109/JSEN.2022.3216578
27 P. J. Rodrigo, M. Lim, and C. Saloma: Opt. Lett. **27** (2002) 25. https://doi.org/10.1364/ol.27.000025
28 J. Bae, J. Park, H. Ahn, and J. Jin: Opt. Express **25** (2017) 12689. https://doi.org/10.1364/oe.25.012689
29 A. D. Rakic, T. Taimre, K. Bertling, Y. L. Lim, P. Dean, A. Valavanis, and D. Indjin: Appl. Phys. Rev. **6** (2019) 19. http://doi.org/10.1063/1.5094674
30 C. M. Jan, C. S. Liu, C. L. Chen, and Y. T. Chen: Opt. Lasers Eng. **145** (2021). https://doi.org/10.1016/j.optlaseng.2021.106668
31 S. Khan, S. Le Calve, and D. Newport: Sens. Actuators, A **302** (2020) 17. https://doi.org/10.1016/j.sna.2019.111782
32 T. D. Nguyen, J. D. R. Valera, and A. J. Moore: Opt. Lasers Eng. **61** (2014) 19. https://doi.org/10.1016/j.optlaseng.2014.04.007
33 J. Park, J. A. Kim, H. Ahn, J. Bae, and J. Jin: Int. J. Precis. Eng. Manuf. **20** (2019) 463. https://doi.org/10.1007/s12541-019-00105-0
34 S. Kim and C. Nguyen: IEEE Trans. Microwave Theory Tech. **52** (2004) 2503. https://doi.org/10.1109/tmtt.2004.837153
35 T. Jaeschke, C. Bredendiek, S. Kuppers, and N. Pohl: IEEE Trans. Microwave Theory Tech. **62** (2014) 3582. http://doi.org/10.1109/tmtt.2014.2365460
36 S. Ayhan, M. Pauli, T. Kayser, S. Scherr, and T. Zwick: 2011 IEEE 8th European Radar Conf. (IEEE, 2011) 117.
37 S. Heining, F. Michler, B. Scheiner, E. Hassan, A. Koelpin, R. Weigel, and F. Lurz: 2020 IEEE Radio and Wireless Symp. (IEEE, 2020) 279.
38 S. Ayhan, S. Scherr, P. Pahl, T. Kayser, M. Pauli, and T. Zwick: IEEE Sens. J. **14** (2014) 734. https://doi.org/10.1109/jsen.2013.2287638
39 Dong Jun Technology, EastWave v6.0 (Dongjun Information Technology Co., Shanghai, 2017).
40 J. R. Aguilar, M. Beadle, P. T. Thompson, and M. W. Shelley: IEE Colloquium on Low Cost Antenna Technology. **206** (1998). http://doi.org/10.1049/ic:19980078
41 D. S. Wilbert, M. P. Hokmabadi, P. Kung, and S. M. Kim: IEEE Trans. Terahertz Sci. Technol. **3** (2013) 846. https://doi.org/10.1109/tthz.2013.2285311
42 F. Costa, S. Genovesi, A. Monorchio, and G. Manara: IEEE Trans. Antennas Propag. **61** (2013) 1201. https://doi.org/10.1109/tap.2012.2227923

About the Authors

Shenwei Yin received his B.S. degree in information & communication engineering from Hunan University, Changsha, China, in 2022. He is currently working toward his Ph.D. degree in electronic science and technology in the School of Physics and Electronics, Hunan University, Changsha, China. His research interests include metamaterials, nonlinear optics, and bound state in the continuum. (yinsw@hnu.edu.cn)

Xiubo Jia received her M. S. degree in materials engineering from Hunan University in 2016. She is now an assistant professor in the School of New Energy, Hunan Vocational Institute of Technology, Xiangtan, China. Her research interest focuses on metamaterial absorbers. (jiaxiubo@xlgy.com)

Jiawen You received her B.S. degree in communication engineering from Hunan University, Changsha, China, in 2022. She is currently working toward her M.S. degree at the University of Electric Science and Technology of China, Chengdu, China. Her research interests include microwave devices for communication applications and antennas. (jiawyou@163.com)

Yuebo Luo received his B.S. degree in communication engineering from Hunan University, Changsha, China, in 2020. He received his M.S. degree in electric engineering from the University of Melbourne, Melbourne, Australia, in 2022. His research interests include metamaterial and antenna. (389865719@qq.com)

Zhixiang Tang received his Ph.D. degree in optical engineering from Shanghai Institute of Optics and Fine Mechanics (SIOM), Chinese Academy of Science (CAS), China, in 2007. He then joined the faculty at Hunan University in Changsha, Hunan Province, China. From Oct. 2013 to Oct. 2014, he was a visiting scholar in the Department of Electrical and Computer Engineering of the National University of Singapore. His research interests include the linear and nonlinear optical properties of man-made nanostructures such as photonic crystals and metamaterials. (tzx@hnu.edu.cn)